

# Multiple-spin coherence transfer in linear Ising spin chains and beyond: numerically-optimized pulses and experiments

Manoj Nimbalkar,<sup>1,\*</sup> Robert Zeier,<sup>1,†</sup> Jorge L. Neves,<sup>1,2</sup> S. Begam Elavarasi,<sup>1,3</sup>  
Haidong Yuan,<sup>4,5</sup> Navin Khaneja,<sup>5</sup> Kavita Dorai,<sup>6</sup> and Steffen J. Glaser<sup>1,‡</sup>

<sup>1</sup>*Department Chemie, Technische Universität München, Lichtenbergstrasse 4, 85747 Garching, Germany*

<sup>2</sup>*Laboratorio de Genômica Estrutural, Instituto de Biofísica Carlos Chagas Filho, Universidade Federal do Rio de Janeiro, Rio de Janeiro RJ 21941-590, Brazil*

<sup>3</sup>*B. S. Abdur Rahman University, Seethakathi Estate, Vandalur, Chennai 600048, India*

<sup>4</sup>*Department of Mechanical Engineering, Massachusetts Institute of Technology, 77 Massachusetts Avenue, Cambridge, MA 02139, USA*

<sup>5</sup>*School of Engineering and Applied Sciences, Harvard University, 33 Oxford Street, Cambridge, MA 02138, USA*

<sup>6</sup>*IISER Mohali, MGSIPAP Complex, Sector 26, Chandigarh 160019, India*

(Dated: October 24, 2011)

We study multiple-spin coherence transfers in linear Ising spin chains with nearest neighbor couplings. These constitute a model for efficient information transfers in future quantum computing devices and for many multi-dimensional experiments for the assignment of complex spectra in nuclear magnetic resonance spectroscopy. We complement prior analytic techniques for multiple-spin coherence transfers with a systematic numerical study where we obtain strong evidence that a certain analytically-motivated family of restricted controls is sufficient for time-optimality. In the case of a linear three-spin system, additional evidence suggests that prior analytic pulse sequences using this family of restricted controls are time-optimal even for arbitrary local controls. In addition, we compare the pulse sequences for linear Ising spin chains to pulse sequences for more realistic spin systems with additional long-range couplings between non-adjacent spins. We experimentally implement the derived pulse sequences in three and four spin systems and demonstrate that they are applicable in realistic settings under relaxation and experimental imperfections—in particular—by deriving broadband pulse sequences which are robust with respect to frequency offsets.

PACS numbers: 82.56.-b, 03.67.Ac, 02.30.Yy

## I. INTRODUCTION

The control of spin dynamics in chains of coupled spins-1/2 is a topic of both theoretical and practical interest [1–12]. On the one hand, the use of spin chains is considered for the efficient transfer of information in future quantum computing devices [13, 14]. On the other hand, coherence transfer between remote spins is the basis of many multi-dimensional experiments for the assignment of complex spectra [15–17] in nuclear magnetic resonance (NMR) spectroscopy. In addition to linear spin chains with only nearest neighbor couplings, in realistic settings also long-range couplings between non-adjacent spins must be considered. For example in <sup>13</sup>C and <sup>15</sup>N labeled proteins, the nuclei in the protein backbone form a chain of coupled spins-1/2 with dominant next neighbor <sup>1</sup>J (single bond) couplings and smaller <sup>2</sup>J and <sup>3</sup>J couplings (via two or three chemical bonds) between non-adjacent spins in the chain [17].

Here we focus on the efficient creation of multi-spin operators from a single-spin operator in a spin chain, such as the creation of multiple-spin order from polarization

of the first spin

$$I_{1z} \rightarrow 2^{n-1} I_{1z} I_{2z} \cdots I_{(n-1)z} I_{nz}. \quad (1)$$

The transfer shown in Eq. (1) is just a prototype example of a general transfer of the form

$$I_{1\delta} \rightarrow 2^{n-1} I_{1\epsilon_1} \cdots I_{n\epsilon_n}, \quad (2)$$

where  $\delta, \epsilon_k \in \{x, y, z\}$  for  $k = 1, \dots, n$ . Note that the transformations in Eqs. (1) and (2) are identical up to local spin rotations. Hence, in the limit where the time for selective rotations of individual spins is negligible (compared to  $1/(2J_{max})$ , where  $J_{max}$  is the largest spin-spin coupling constant in the chain), the transformations in Eqs. (1) and (2) can be achieved in the same amount of time. (This situation is typical for heteronuclear NMR experiments in liquid state, where the control amplitudes for single spin operators are orders of magnitude larger than the largest coupling constants.) In Eq. (2), the initial single-spin state is not limited to longitudinal magnetization (polarization  $I_{1z}$ ) but may also be transverse magnetization (in-phase coherence  $I_{1x}$  or  $I_{1y}$ ) [17, 18]. Examples of multi-spin target operators in Eq. (2) containing one or several transverse operators include states of the form  $2^{n-1} I_{1z} I_{2z} \cdots I_{(n-1)z} I_{nx}$  (corresponding to anti-phase coherence of spin  $n$  with respect to spins 1 to  $n-1$ ), and  $2^{n-1} I_{1x} I_{2x} \cdots I_{(n-1)x} I_{nx}$  (corresponding to multi-quantum coherence), which are relevant in so-called “out and back” transfer schemes [17, 19, 20] and

\* manoj.nimbalkar@tum.de

† robert.zeier@ch.tum.de

‡ steffen.glaser@tum.de

in the creation of multiple-quantum coherence [18, 21], respectively.

We consider the case of Ising-type spin chains [22, 23], corresponding to the weak coupling limit [18]. In this limit, which is an excellent approximation for hetero-nuclear NMR experiments, the coupling Hamiltonian for a pair of spins  $k$  and  $l$  has the form

$$H_{kl}^{\text{weak}} = 2\pi J_{kl} I_{kz} I_{lz},$$

where  $J_{kl}$  is the coupling constant in units of Hertz (Hz). In conventional experiments, the standard methods to achieve transfer in Eq. (2) are based on COSY- or RELAY-type transfer steps [17, 18], which are realized in hetero-nuclear experiments by a series of INEPT building blocks [24] (see Sec. II). The transfer time is determined by the size of the coupling constants  $J_{kl}$  in a given spin system. For example, in a linear spin chain with only next-neighbor couplings, the total duration is given by

$$T_{\text{conv}} = (J_{12}^{-1} + J_{23}^{-1} + \dots + J_{(n-1)n}^{-1})/2.$$

We are interested in finding the shortest possible time to achieve the transfer in Eq. (2) or conversely, the maximum transfer amplitude for any given time, which remains an open question up to now.

For relatively simple spin systems, consisting of up to three spins, time-optimal [25–31] and relaxation-optimized [32–37] pulse sequences have been recently found analytically based on methods of optimal control theory [38–42], establishing rigorous physical limits of minimal transfer times or minimal relaxation losses, respectively. In addition to powerful analytical tools, optimal control theory also provides efficient numerical algorithms for the optimization of pulse sequences, such as the gradient ascent pulse engineering (GRAPE) algorithm, exploiting the known equation of motion for the spin system [43–46]. With this algorithm it is possible to optimize tens of thousands of pulse sequence parameters and the resulting pulse sequences are not limited to previously known transfer schemes. However, in contrast to analytical methods proving global optimality of a given pulse sequence, there is no guarantee that numerical optimal control algorithms like GRAPE will converge to the global optimum [47]. Never-the-less, in cases where the theoretical limits are known, the GRAPE algorithm closely approached these limits [43, 48]. This motivated its use also in cases for which analytical results on the global optimum are presently unknown in order to explore the physical limits of the maximum possible transfer efficiency as a function of transfer time, resulting in so-called TOP (time-optimal pulse) curves [41, 49–53]. Furthermore, additional effects such as relaxation [54, 55], radiation damping [56], and experimental constraints and imperfections—such as limited control amplitudes and control field inhomogeneities [57–59]—can be taken into account to find highly robust pulses suitable for practical applications under realistic conditions.

Assuming a restricted pulse structure (see Secs. III A and IV A) analytic pulses were derived in Refs. [11] and [12], respectively, for the case of equal and unequal couplings. This results in significantly shorter transfer times compared to conventional approaches, however it was not clear how closely the performance of the derived pulse sequences converges to the time-optimal performance.

In this work, we summarize the analytic approach of Refs. [11, 12] (see Sections III A and IV A) and explore its time-optimality by conducting a systematic numerical study of the considered coherence transfer (see Sections III B and IV B). Focusing on the case of linear Ising spin chains with three and four qubits we compare the duration of pulse sequences for arbitrary pulse structures with the restricted pulse structure motivated by the analytic pulses. We also numerically analyze linear Ising spin chains for up to six spins (see Section VII). In addition, our numerical approach makes it also possible to investigate more realistic spins systems with more general coupling topologies (see Section V).

In Sec. VI, we show how to make the pulse sequences robust with respect to off-resonance effects using the DANTE (Delays Alternating with Nutations for Tailored Excitation) approach [29, 60, 61]. Finally, we present experimental results for model spin chains consisting of three and four hetero-nuclear spins-1/2, demonstrating good performance of the new sequences under experimental conditions and comparing the results to conventional pulse sequences.

## II. COHERENCE TRANSFER IN LINEAR ISING SPIN CHAINS

Throughout this work we mostly consider linear Ising spin chains which have only direct couplings between neighboring spins [22, 23]. (Later we will also allow additional couplings between non-neighboring spins.) Assume that a chain of  $n$  spins is placed in a static external magnetic field along the  $z$ -direction and that neighboring spins are coupled by an Ising interaction where the coupling strengths  $J_{\ell, \ell+1}$  are fixed but may depend on the position  $1 \leq \ell \leq n-1$  in the chain. Without any control, the system evolves freely under its drift Hamiltonian

$$H_d = 2\pi \sum_{l=1}^{n-1} J_{l, l+1} I_{lz} I_{(l+1)z}.$$

The drift Hamiltonian is given in a suitably chosen multiple rotating frame, which rotates simultaneously at the resonance frequency of each spin. We use the product-operator basis  $I_{\ell\nu} = \bigotimes_j I_{a_j}$  where  $a_j = \nu$  for  $j = \ell$  and  $a_j = 0$  otherwise (see Ref. [18]). The matrices  $I_x := (\begin{smallmatrix} 0 & 1 \\ 1 & 0 \end{smallmatrix})/2$ ,  $I_y := (\begin{smallmatrix} 0 & -i \\ i & 0 \end{smallmatrix})/2$ , and  $I_z := (\begin{smallmatrix} 1 & 0 \\ 0 & -1 \end{smallmatrix})/2$  are the Pauli spin matrices and  $I_0 := (\begin{smallmatrix} 1 & 0 \\ 0 & 1 \end{smallmatrix})$  is the  $(2 \times 2)$ -dimensional identity matrix. In addition to the free evolution, we assume that individual spins can be selectively excited using radio-frequency (rf) pulses, which is the case if the Larmor

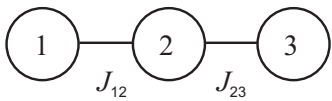


FIG. 1. A linear three-spin chain has only direct couplings  $J_{12}$  and  $J_{23}$  between neighboring spins.

frequencies of the spins are well separated as compared to the coupling strengths  $J_{\ell,\ell+1}$ . Thus controls on individual spins can be applied on a much faster time scale as compared to the free evolution w.r.t. the drift Hamiltonian.

We derive explicit controls for the amplitude and phase of the external rf fields implementing a unitary evolution which transforms an initial polarization  $I_{1x}$  on the first spin to a multiple-spin state  $2^{n-1}(\prod_{\ell=1}^{n-1} I_{\ell y})I_{nz}$  while minimizing the pulse duration  $t_p$ . In the following, we often compare control pulses with the *conventional strategy*, which consists of  $n-1$  steps of free evolution ( $1 \leq m \leq n-1$ )

$$2^{m-1}I_{1y} \cdots I_{m-1,y}I_{mx} \xrightarrow{H_d} 2^m I_{1y} \cdots I_{my}I_{m+1,z}$$

where each individual step—besides the final one—is followed by one hard  $\frac{\pi}{2}$ -pulse on the  $(m+1)$ th spin along the  $y$ -direction. As each period of free evolution is of length  $1/(2J_{\ell,\ell+1})$  where  $J_{\ell,\ell+1}$  is given in Hz, the total evolution time is given by  $t_p = \sum_{\ell=1}^{n-1} 1/(2J_{\ell,\ell+1})$ .

### III. LINEAR THREE-SPIN CHAINS: ANALYTIC AND NUMERICAL APPROACHES

#### A. Analytic approach

In this section, we consider the model of Sect. II in the case of linear three-spin chains (see Fig. 1). In the most general case, one could allow independent controls on each of the three spins along both the  $x$ - and  $y$ -direction. But in order to simplify the control problem we allow only one control on the second spin along the  $y$ -direction. This might not lead to time-optimal controls. But even using this restricted model, controls which are shorter as compared to the conventional strategy were obtained in Ref. [12] (see also [11]). In the following, we summarize the analytical approach of Ref. [12].

Starting from an initial state  $I_{1x}$  and using only one control on the second spin along the  $y$ -direction, we can analyze the control problem on the subspace spanned by the operators  $I_{1x}$ ,  $2I_{1y}I_{2z}$ ,  $2I_{1y}I_{2x}$ , and  $4I_{1y}I_{2y}I_{3z}$  as compared to the full 63-dimensional space of operators. Using the notation  $\langle O \rangle := \text{Tr}(O\rho)$  for the expectation value and  $\text{Tr}$  for the trace, we denote the corresponding expectation values by  $x_1 = x_1(t) = \langle I_{1x} \rangle$ ,  $x_2 = x_2(t) = \langle 2I_{1y}I_{2z} \rangle$ ,  $x_3 = x_3(t) = \langle 2I_{1y}I_{2x} \rangle$ , and  $x_4 = x_4(t) = \langle 4I_{1y}I_{2y}I_{3z} \rangle$ . We obtain the differential

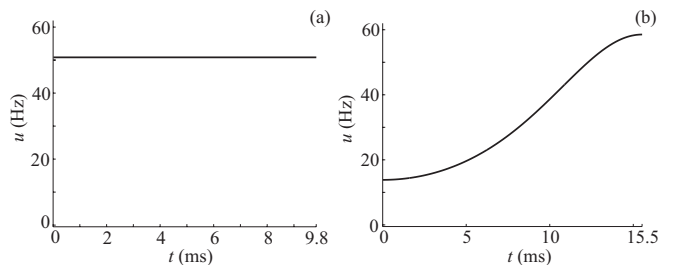


FIG. 2. Analytic pulses for linear three-spin chains are given in the cases of (a)  $k = J_{23}/J_{12} = 88.05/88.05 = 1$  and (b)  $k = 1.59 \approx J_{23}/J_{12} = 73.1/46$ .

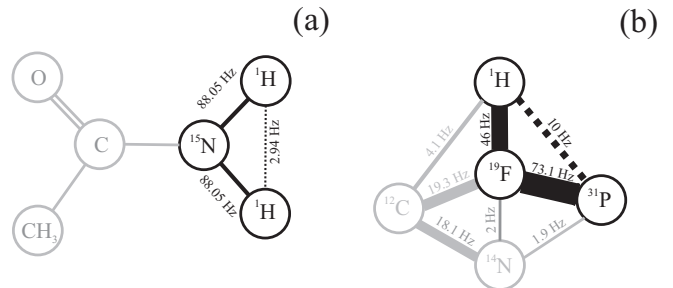


FIG. 3. The schematic coupling topologies of (a) ethanamide and (b) diethyl-(dimethylcarbonyl)fluoromethylphosphonate (see [62, 63]) result in experimental three-spin systems with coupling ratios (a)  $k = 1 = 88.05/88.05$  and (b)  $k = 1.59 \approx 73.1/46$ . Larger couplings are shown as solid-black lines, and smaller couplings are shown as dashed-black lines. Decoupled spins are given in gray color.

equation

$$\begin{pmatrix} \dot{x}_1 \\ \dot{x}_2 \\ \dot{x}_3 \\ \dot{x}_4 \end{pmatrix} = \pi \begin{pmatrix} 0 & -1 & 0 & 0 \\ 1 & 0 & -u & 0 \\ 0 & u & 0 & -k \\ 0 & 0 & k & 0 \end{pmatrix} \begin{pmatrix} x_1 \\ x_2 \\ x_3 \\ x_4 \end{pmatrix}, \quad (3)$$

where  $u = u(t)$  denotes the amplitude of the control on the second spin along the  $y$ -direction and  $k = J_{23}/J_{12}$ . Using the coordinates  $(x_1, x_2, x_3, x_4)^T$  we aim to time-efficiently transfer  $(1, 0, 0, 0)^T$  to  $(0, 0, 0, 1)^T$ .

Now, we change from the coordinates  $(x_1, x_2, x_3, x_4)^T$  to the coordinates

$$(r_1, r_2, r_3)^T = (x_1, \sqrt{x_2^2 + x_3^2}, x_4)^T$$

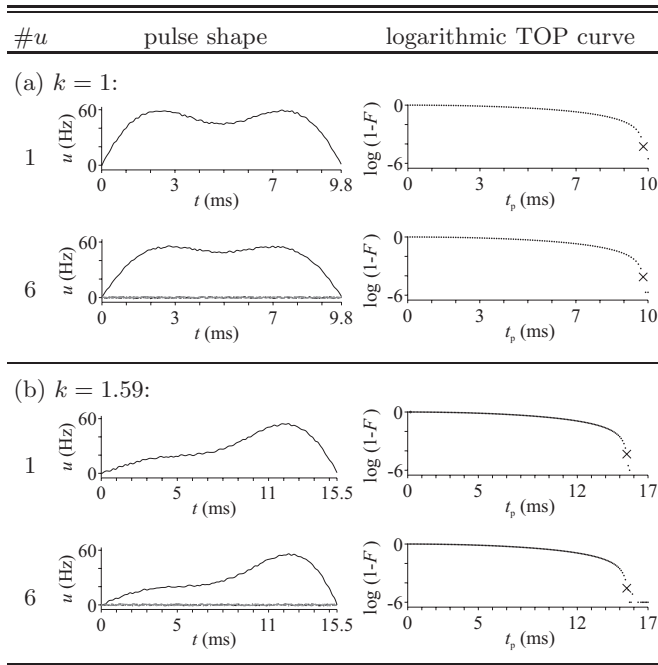
on the sphere where  $\theta = \theta(t)$  is given by  $\tan \theta = x_3/x_2$ . This transforms Eq. (3) to

$$\begin{pmatrix} \dot{r}_1 \\ \dot{r}_2 \\ \dot{r}_3 \end{pmatrix} = \pi \begin{pmatrix} 0 & -\cos \theta & 0 \\ \cos \theta & 0 & -k \sin \theta \\ 0 & k \sin \theta & 0 \end{pmatrix} \begin{pmatrix} r_1 \\ r_2 \\ r_3 \end{pmatrix}.$$

In the new coordinates, we want to time-efficiently transfer  $(1, 0, 0)^T$  to  $(0, 0, 1)^T$ .

In order to find the time-optimal controls, Euler-Lagrange equations were set up and solved in Ref. [12]

TABLE I. We compare the duration  $t_p$ , the logarithmic fidelity  $F$ , and the shape of numerically-optimized pulses for a linear three-spin chain with coupling ratios (a)  $k = 1$  and (b)  $k = 1.59$ . The number of controls  $\#u$  is given in the first column. In the third column we present the corresponding logarithmic TOP curves. The second column shows an example of a shaped pulse, whose position is denoted with an x in the logarithmic TOP curve. The rf control on the middle spin along the  $y$ -axis is plotted using a solid-black line. Other rf controls are plotted using dashed or solid-gray lines.



leading to the differential equation

$$\ddot{\theta} = \frac{k^2 - 1}{2} \sin 2\theta \quad (4)$$

for the variable  $\theta$ . The differential Eq. (4) can be numerically integrated if the initial values  $\theta(0)$  and  $\dot{\theta}(0)$  are known. Using the results of Ref [12] one can determine conditions on the initial values: In the case of  $(r_1(0), r_2(0), r_3(0))^T = (1, 0, 0)^T$  one can deduce that  $\theta(0) = 0$ , but  $\dot{\theta}(0)$  is undetermined. In Ref. [12] combinations of one-dimensional searches were used to determine the optimal  $\theta_{\text{opt}}(t)$  and the time-optimized control as  $u_{\text{opt}}(t) = J_{12}\dot{\theta}_{\text{opt}}(t)$ . Examples for the corresponding (semi-)analytic pulses are shown in Fig. 2. The values are motivated by the experimental systems given in Fig. 3.

## B. Numerical approach

We numerically optimize pulse shapes by employing the GRAPE algorithm [43] which was developed by employing principles of optimal control theory. Using a gradient-based optimization we obtain rf controls which

TABLE II. For coherence transfers in linear three-spin chains ( $k = 1$  and  $k = 1.59$ ), we give the numerically-optimized times  $t_p$  and the fidelities  $F$  in the case of one, two, and six rf controls (see text). The duration  $t_p$  is independent of the number of controls which suggests that only one rf-control on the middle spin is sufficient for the time-optimal coherence transfer.

$k$	$\#u$	$t_p$ (s)	$F$	$k$	$\#u$	$t_p$ (s)	$F$
1	1	0.0098	0.9999	1.59	1	0.0155	0.9999
1	2	0.0098	0.9999	1.59	2	0.0155	0.9999
1	6	0.0098	0.9999	1.59	6	0.0155	0.9999

steer an initial state (or unitary transformation) to a final state (or unitary transformation) while minimizing (e.g.) the duration of the pulse. Both the amplitude and the phase of the resulting pulse can be smoothly- or noisily-shaped depending on e.g. the initial pulse or bounds on the control strength (see, e.g. [58]).

We treat three different levels of rf controls: First, we use only one rf control operating on the second spin along the  $y$ -direction. Second, we use two different rf controls operating on the second spin along both the  $x$ - and  $y$ -direction. Third, we use a total of six rf controls operating on each of the three spins along both the  $x$ - and  $y$ -direction. We remark that employing rf controls on one spin along both the  $x$ - and  $y$ -direction gives complete (local) control on that spin. Let  $k$  denote the ratio between the couplings  $J_{23}$  and  $J_{12}$ . We determine the numerically-optimized pulses and plot the logarithmic fidelity  $F$  vs. the duration  $t_p$  of different shaped pulses for the coupling ratios  $k = 1$  and  $k = 1.59$  which are motivated by the experimental scenarios of Fig. 3. The numerical results are given in Table I: We show examples of shaped pulses with short duration  $t_p$  and high fidelity  $F \geq 0.9999$ . In addition, we present logarithmic time-optimal (TOP) curves where we plot the logarithmic transfer efficiency (i.e.  $\log(1-F)$  where  $F$  is the fidelity) versus the optimal transfer time. Comparing the different cases suggests that only one rf control on the second spin is sufficient for a time-optimal pulse. For high fidelities ( $F \geq 0.9999$ ), the durations of the analytic and numerically-optimized pulses are identical (in the given accuracy) while the pulse forms differ. In Table II, we compare the duration of pulses on linear three-spin systems for different values of  $k$ .

**Conjecture 1** Consider a linear three-spin chain with local controls on each spin. One can time-optimally transfer coherence from  $I_{1x}$  to  $4I_{1y}I_{2y}I_{3z}$  using only one control on the second spin along the  $y$ -direction. In addition, the analytical pulses of Refs. [11, 12] are time-optimal in the case of linear three-spin chains even if one allows arbitrary local controls.

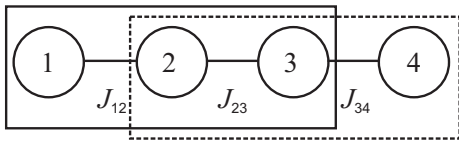


FIG. 4. A linear four-spin chain has only direct couplings  $J_{12}$ ,  $J_{23}$ , and  $J_{34}$  between neighboring spins. We split the corresponding four-spin chain control problem into two subproblems for three-spin chains.

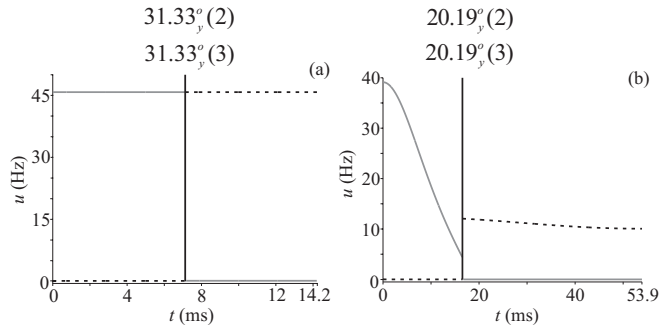


FIG. 5. Analytic pulses for linear four-spin chains are given in the cases of (a)  $k_1 = k_2 = 1$  as well as (b)  $k_1 = 2.38$  and  $k_2 = 0.94$ . The pulses on the second and third spin along the  $y$ -direction are given, respectively, as solid and dashed line. The corresponding two hard pulses on the second and third spin are depicted by a vertical line where the flip angles are given above. The hard pulses in the left figure can be implemented by applying a pulse of 5000 Hz for 17.40 microseconds. The hard pulses in the right figure can be implemented by applying a pulse of 5000 Hz for 11.21 microseconds.

#### IV. LINEAR FOUR-SPIN CHAINS: ANALYTIC AND NUMERICAL APPROACHES

##### A. Analytic approach

In this section, we consider linear spin chains with four spins. We follow Sect. IV of Ref. [12] (see also [11]) and split the control problem for four spins into two subproblems for three spins (see Fig. 4): The first subproblem is given on the first three spins by the time-optimal transfer from  $(1, 0, 0)^T$  to  $(0, \cos \gamma, \sin \gamma)^T$ , where we are again using the coordinates  $(r_1, r_2, r_3)^T$  of Sect. III A. Then, we apply certain (arbitrarily fast) hard pulses which can be easily determined by numerical methods. The second subproblem is given on the last three spins by the time-optimal transfer from  $(\cos \gamma, \sin \gamma, 0)^T$  to  $(0, 0, 1)^T$ . In addition, we have to simultaneously search for the value of  $\gamma$  which minimizes the pulse duration. This approach might not lead to time-optimal controls but simplifies the control problem significantly.

The optimization of the considered subproblems can be reduced to time-optimal transfers from  $(\cos \alpha, \sin \alpha, 0)^T$  to  $(0, \cos \beta, \sin \beta)^T$  for  $\alpha, \beta \in [0, \pi/2]$  generalizing the transfer of Sect. III A from  $(1, 0, 0)^T$  to  $(0, 0, 1)^T$ . Using methods of Ref. [12] we can find the optimal con-

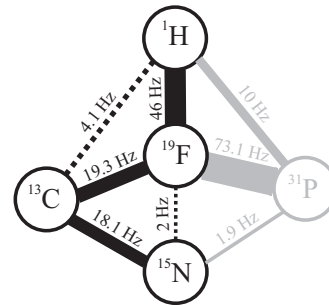


FIG. 6. The topology of the molecule  $^{13}\text{C}^{\text{O}}\text{-}^{15}\text{N}$ -diethyl-(dimethylcarbonyl)fluoromethylphosphonate (see [62, 63]) results in coupling ratios  $k_1 = 2.38$  and  $k_2 = 0.94$ . Compare to Fig. 3.

trols for the transfers using combined one-dimensional searches for the optimal initial values  $\theta(0)$  and  $\dot{\theta}(0)$  of Eq. (4). Both  $\theta(0)$  and  $\dot{\theta}(0)$  are undetermined but related by  $\dot{\theta}(0) = \sin[\theta(0)] \cot \alpha$  for the case of  $(r_1(0), r_2(0), r_3(0))^T = (\cos \alpha, \sin \alpha, 0)^T$ . The corresponding (semi-)analytic pulses are shown in Fig. 5. The values are motivated by the experimental system given in Fig. 6.

##### B. Numerical approach

Motivated by the analytical approach, we numerically treat the control problem on four spins with two cases of coupling ratios (a)  $k_1 = 1$  and  $k_2 = 1$  ( $J_{12} = J_{23} = J_{34} = 88.05$  Hz), and (b)  $k_1 = 2.38 \approx J_{12}/J_{23}$  and  $k_2 = 0.94 \approx J_{34}/J_{23}$  (refer to Fig. 6 for the coupling values). The coherence transfer is numerically optimized considering the following three levels of rf controls: First, we use only two different rf controls (one on each spin) operating on the second and third spin along the  $y$ -direction. Second, we use a total of four different rf controls (two on each spin) operating on the second and third spin along both the  $x$ - and  $y$ -direction. Third, we use a total of eight different rf controls (two on each spin) operating on each of the four spins along both the  $x$ - and  $y$ -direction. The pulse shapes and the logarithmic TOP curves corresponding to two and eight rf controls (see Table III) indicate that we do not gain a higher fidelity or a shorter duration from using more than the two controls (Table IV). This is consistent with the analytic results, but the numerically-optimized pulses appear to be a little shorter than the analytical ones (cp. Fig. 5).

**Conjecture 2** Consider a linear four-spin chain with local controls on each spin. One can time-optimally transfer coherence from  $I_{1x}$  to  $8I_{1y}I_{2y}I_{3y}I_{4z}$  using only two controls along the  $y$ -direction which operate on the second and third spin, respectively.

TABLE III. For linear four-spin chains with coupling ratios (a)  $k_1 = 1$  and  $k_2 = 1$  as well as (b)  $k_1 = 2.38$  and  $k_2 = 0.94$ , the rf controls on the second and third spin along the  $y$ -axis are plotted using solid-black and solid-gray lines, respectively. Other rf controls are plotted using a dashed-black line or in shades of gray. Compare to Table I.

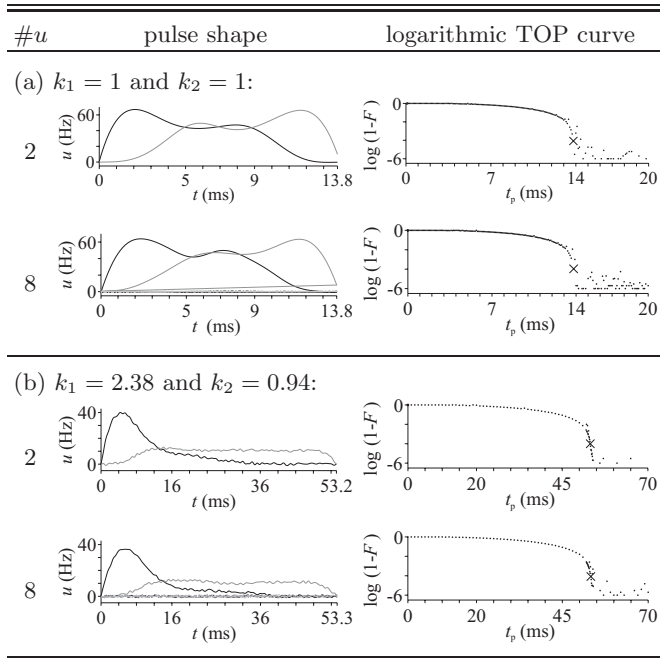


TABLE IV. For coherence transfers in linear four-spin chains ( $k_1 = k_2 = 1$  as well as  $k_1 = 2.38$  and  $k_2 = 0.94$ ), we give the numerically-optimized times  $t_p$  and the fidelities  $F$  in the case of two, four, and eight rf-controls. The duration  $t_p$  is independent of the number of controls which suggests that only two rf-control on the second and third spin along the  $y$ -axis is sufficient for the time-optimal coherence transfer.

$k_1$	$k_2$	$\#u$	$t_p$ (s)	$F$	$k_1$	$k_2$	$\#u$	$t_p$ (s)	$F$
1	1	2	0.138	0.9999	2.38	0.94	2	0.532	0.9999
1	1	4	0.138	0.9999	2.38	0.94	4	0.532	0.9999
1	1	8	0.138	0.9999	2.38	0.94	8	0.533	0.9999

## V. MORE GENERALLY-COUPLED SPIN SYSTEMS OF THREE AND FOUR SPINS

In more generally-coupled spin systems, indirect couplings can strongly impede or enhance the coherence transfer. In this section we present detailed numerical optimizations and compare them to the case of linear spin chains.

### A. Three-spin system

Along the lines of Section III B, we numerically optimize pulses for more generally-coupled three-spin sys-

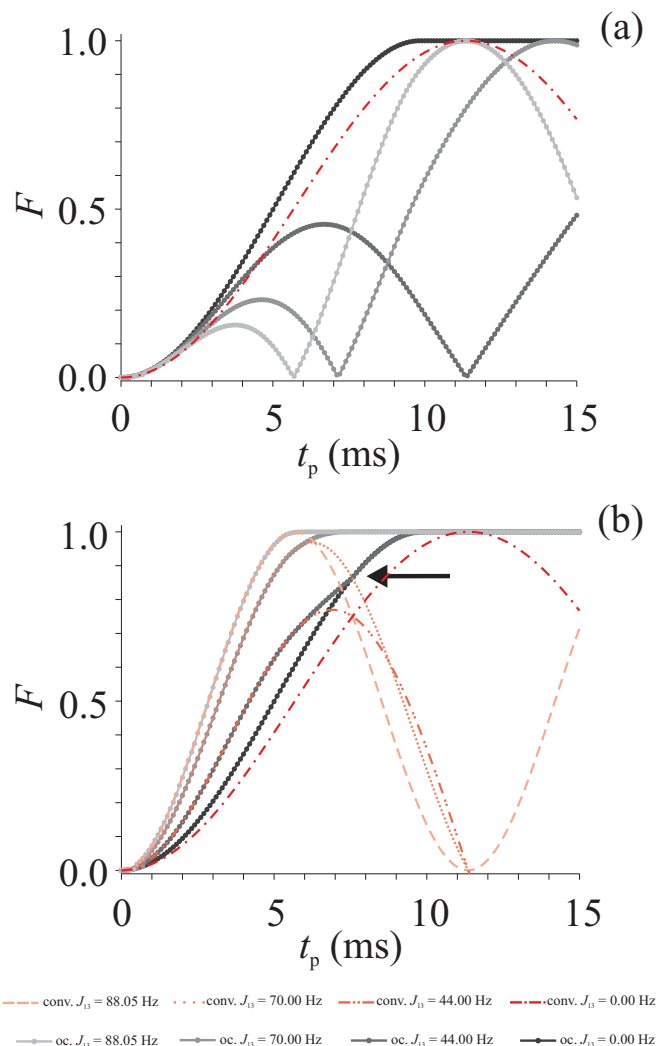
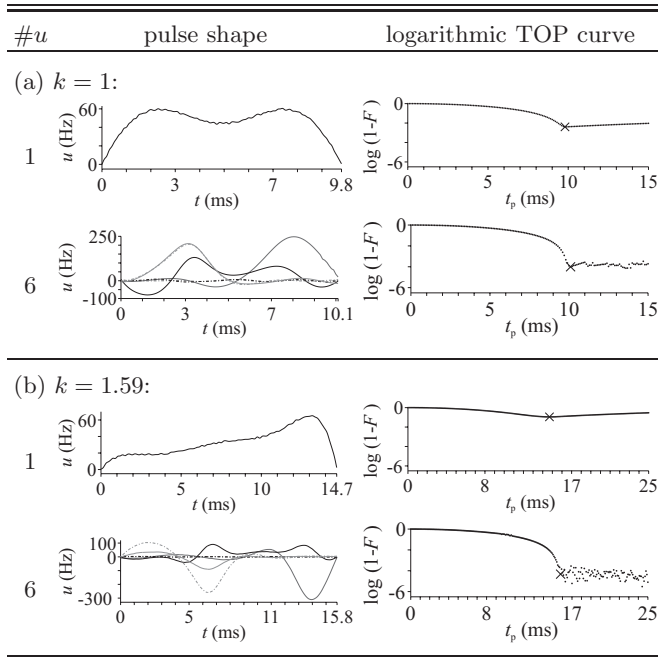


FIG. 7. (Color online) We compare numerically-optimized TOP curves (in shades of gray) for three-spin systems with one [Subfigure (a)] and six [Subfigure (b)] rf controls keeping  $J_{12} = J_{23} = 88.05$  Hz constant while varying  $J_{13}$ . At the same time we compare their performance with conventional pulse sequences (in shades of red) where both of the couplings  $J_{12}$  and  $J_{13}$  evolve simultaneously. The limiting case of  $J_{13} = 0$  corresponds to the conventional pulse sequence of Sec. II. Using all six rf controls [Subfigure (b)] we can see higher fidelities  $F$  for smaller times and larger  $J_{13}$  compared to the case of only one rf control [Subfigure (a)]. A black arrow denotes where the numerically-optimized TOP curves for  $J_{13} = 44$  Hz and  $J_{13} = 0$  Hz merge.

tems keeping  $J_{12} = J_{23} = 88.05$  Hz constant while varying the additional coupling strength  $J_{13}$ . By comparing the TOP curves for different values of  $J_{13}$ , we conclude that for a larger coupling strength  $J_{13}$  the fidelity of the coherence transfer is smaller in the cases of one [Fig. 7(a)] and two (results are not shown) rf controls on the second spin. (As in Section III B, we obtain shorter pulse sequences as compared to the conventional pulse sequence for  $J_{13} = 0$ .) However, using the rf controls on each

TABLE V. Numerical results for more generally-coupled three-spin systems with (a) coupling ratio  $k = 1$  (i.e.  $J_{12} = J_{23} = 88.05$  Hz) and additional coupling  $J_{13} = 2.935$  Hz as well as (b) coupling ratio  $k = 1.59$  (i.e.  $J_{12} = 73.1$  Hz and  $J_{23} = 46$  Hz) and additional coupling  $J_{13} = 10.0$  Hz. Compare to Table I.



of the three spins allows for a coherence transfer with higher fidelity while keeping the pulses short [Fig. 7(b)]. Table V shows examples of shaped pulses and the corresponding logarithmic TOP curves for the coupling ratios  $k = 1$  and  $k = 1.59$ . The coupling strengths are taken from the spin systems shown in Fig. 3. Detailed values are given in Table VII.

### B. Four-spin system

Following Section IV B, we numerically optimize the shaped pulses for a more generally-coupled four-spin systems. Analyzing the numerical results (see Table VI), we can say that this system needs all eight rf controls on each spin along both the  $x$ - and  $y$ -direction in order to achieve the coherence transfer with minimum duration and maximal fidelity. Table VII summarizes and compares the duration  $t_p$  and fidelity  $F$  of shaped pulses for more generally-coupled spin systems.

## VI. EXPERIMENTAL RESULTS

Analytic and numerically-optimized pulses are usually optimized for on-resonance cases. We follow the DANTE approach [60, 61, 64] in order to obtain pulses which are broadband, i.e. invariant with respect to the change of

TABLE VI. Numerical results for a more generally-coupled four-spin systems with coupling ratios  $k_1 = 2.38 \approx J_{12}/J_{23}$  and  $k_2 = 0.94 \approx J_{34}/J_{23}$  (i.e.  $J_{12} = 46$  Hz,  $J_{23} = 19.3$  Hz, and  $J_{34} = 18.1$  Hz) as well as additional couplings  $J_{13} = 4.1$  Hz and  $J_{24} = 2$  Hz. Compare to Table III.

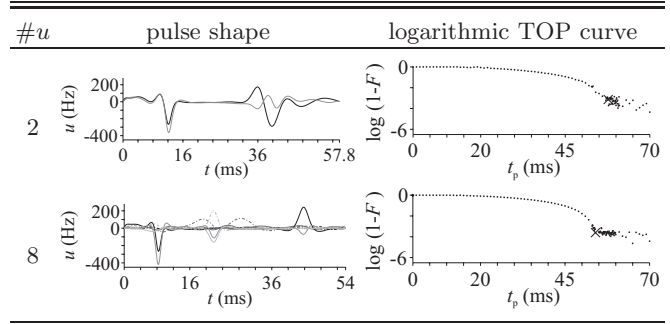


TABLE VII. We compare the duration  $t_p$  and fidelity  $F$  of numerically-optimized shaped pulses in the case of three- and four-spin systems allowing a varying number of rf controls  $u$ . Using only one rf control we show the effect of indirect couplings—which are usually present in experiments—on the fidelity of optimized pulses. Hence more rf controls are necessary for higher fidelities. The  $J$ -values are taken from the actual spin systems shown in Figs. 3 and 6.

graph	$J_{13}$ (Hz)	$J_{24}$ (Hz)	$\#u$	$t_p$ (ms)	$F$
$k = 1$					
	0.0	–	1	9.8	0.9999
	2.9	–	1	9.8	0.9959
	2.9	–	6	11.5	0.9999
$k = 1.59$					
	0.0	–	1	15.5	0.9999
	10.0	–	1	15.5	0.8837
	10.0	–	6	15.8	0.9999
$k_1 = 2.38$ and $k_2 = 0.94$					
	0.0	0.0	2	53.2	0.9999
	4.1	2.0	2	53.2	0.9859
	4.1	2.0	8	54.0	0.9999

the chemical shift in a given offset range (Fig. 8). First, a shaped pulse is converted into a sequence of short hard pulses and delays. We used hard pulses with constant flip angles (see below), and the delays between the hard pulses correspond to the time required by the shaped pulse to accumulate this flip angle [60, 61, 64]. Then, a refocusing element (i.e.  $\pi$ -pulse) [29, 61] is inserted between two hard pulses. The offset bandwidth covered by a refocused DANTE sequence is directly proportional to the rf amplitude of the hard pulses and the  $\pi$ -pulses used in the sequence.

All the experiments are implemented on a Bruker AVANCE III 600 MHz spectrometer at 298 Kelvin: We use a triple resonance TXI probe head with Z-gradient in the case of the three-spin system with  $k = 1$ . For the

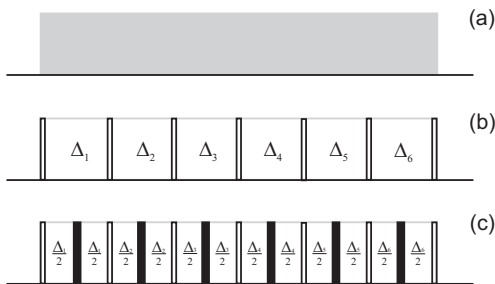


FIG. 8. In the DANTE approach an on-resonance shaped pulse (see (a)) is converted to a series of short hard pulses and delays  $\Delta_i$  (see (b)). Then, the pulse can be converted to a broadband pulse by inserting a refocusing element (i.e.  $\pi$ -pulse) represented by solid bars between two hard pulses (see (c)).

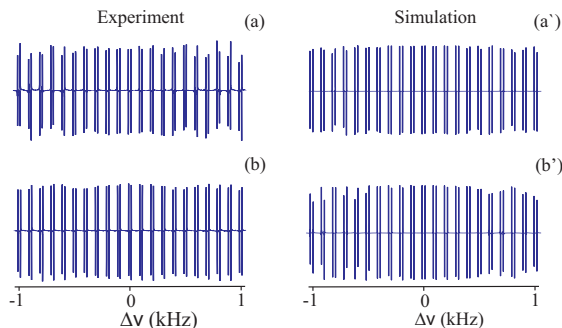


FIG. 9. (Color online) We compare for a three-spin system the offset ( $\Delta v$ ) profile for  $\pm 1$  kHz of the anti-phase signal (see text) resulting from a conventional pulse sequence ( $t_p = 11.4$  ms) in the case of experiment (see (a)) and simulation (see (a')) with broadband versions of the analytic pulses ( $t_p = 9.8$  ms, see (b) and (b')) for the case of coupling ratio  $k = 1$  of three spins.

three spin system with  $k = 1.59$  and the four spin system with  $k_1 = 2.38$  and  $k_2 = 0.94$  we use a custom-made 6-channel probe head with Z-gradient addressing all nuclei  $^{19}\text{F}$ ,  $^1\text{H}$ ,  $^{31}\text{P}$ ,  $^{12}\text{C}$  (or  $^{13}\text{C}$ ), and  $^{14}\text{N}$  (or  $^{15}\text{N}$ ) (see [62, 63]). In the experiments for three spins we use the molecules shown in Fig. 3. The experiment for the coupling ratio  $k = 1$  uses the first molecule (see Fig. 3(a)) which is dissolved in deuterated water  $\text{D}_2\text{O}$ . For  $k = 1.59$  we use the second molecule (see Fig. 3(b)) dissolved in deuterated methanol  $\text{CD}_3\text{OD}$ . The simulated and experimental offset profiles are shown in Figs. 9 and 10. We emphasize that the duration of the broadband versions of the analytic or the numerically-optimized pulses is shorter than for the conventional pulse sequence while keeping its robustness.

We first discuss two three-spin systems: In the case of  $k = 1$ , we start from the initial polarization  $I_{1z}$  of  $^1\text{H}$  (which models the first spin) and apply a  $\frac{\pi}{2}$ -pulse along  $+y$ -direction in order to obtain the coherence  $I_{1x}$ . By applying a broadband version of our shaped pulse of  $^{15}\text{N}$  (which models the second spin) we get the three-

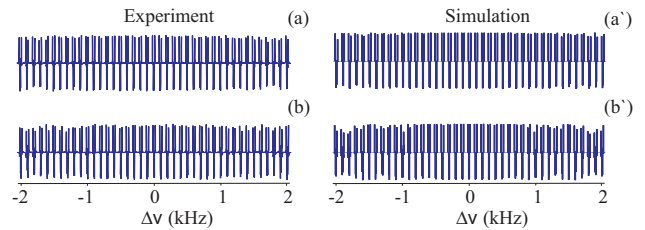


FIG. 10. (Color online) We compare for a three-spin system the offset ( $\Delta v$ ) profile for  $\pm 2$  kHz of the anti-phase signal (see text) resulting from a conventional pulse sequence ( $t_p = 17.7$  ms) in the case of experiment (see (a)) and simulation (see (a')) with broadband versions of the analytic pulses ( $t_p = 15.5$  ms, see (b) and (b')) for the case of coupling ratio  $k = 1.59$ .

spin coherence  $4I_{1y}I_{2y}I_{3z}$ . The broadband version of this shaped pulse is divided into four hard pulses with an amplitude of 4145.936 Hz, a flip angle of 45.00 degrees, and zero phase; it also contains refocusing  $\pi$ -pulses where the phases are chosen according the MLEV-4 cycle [65]. Next, we apply  $\frac{\pi}{2}$ -pulse on  $^{15}\text{N}$  along the  $x$ -direction and we obtain the coherence  $4I_{1y}I_{2z}I_{3z}$ . In the end, we can detect an anti-phase signal of  $^1\text{H}$  (first spin) with respect to the spins of  $^{15}\text{N}$  and  $^1\text{H}$  (which models the third spin). Similarly, in the case of  $k = 1.59$ , we start from the initial coherence  $I_{1z}$  on the spin of  $^1\text{H}$  (which models the first spin) and apply a  $\frac{\pi}{2}$ -pulse along  $+y$ -direction in order to obtain the coherence  $I_{1x}$ . Then, we apply the broadband version of our shaped pulse on the spin of  $^{19}\text{F}$  in order to produce the three-spin coherence  $4I_{1y}I_{2y}I_{3z}$ . The broadband version of this shaped pulse is divided into four hard pulses with an amplitude of 10000 Hz, a flip angle of 45.03 degrees, and zero phase; it also contains refocusing  $\pi$ -pulses where the phases are chosen according the MLEV-4 cycle [65]. In the next step, we apply a  $\frac{\pi}{2}$ -pulse on the spin of  $^1\text{H}$  and we end up with the coherence  $4I_{1z}I_{2y}I_{3z}$ . Finally, we detect an anti-phase signal on the spin of  $^{19}\text{F}$  with respect to the spins of  $^1\text{H}$  and  $^{31}\text{P}$ .

In the four-spin system, we show on-resonance simulations and experiments for numerically-optimized shaped pulses comparing the conventional approach with analytical and numerically-optimized pulses (see Fig. 11). The corresponding experiments are implemented on the molecule of Fig. 6, which is dissolved in deuterated acetonitrile. Figures 11(b) and (c) show a reduction in signal intensity for the simulation if we compare the effect of the pulse on the abstract linear spin chain (shown in gray) with the effect on the more realistic and more generally-coupled spin system (shown in black) as the corresponding pulses were only optimized for the abstract linear spin chain. We remark that the pulse of Fig. 11(d) is optimized for a more generally-coupled spin system while using rf-controls on all spins. Thus, we conclude—using also the data of Table VII—that the pulse of Fig. 11(d) shows a higher fidelity when compared to the pulses of Figs. 11(b) and (c). Furthermore, the pulse corresponding to Fig. 11(d) is shorter (by 14%) than the conven-

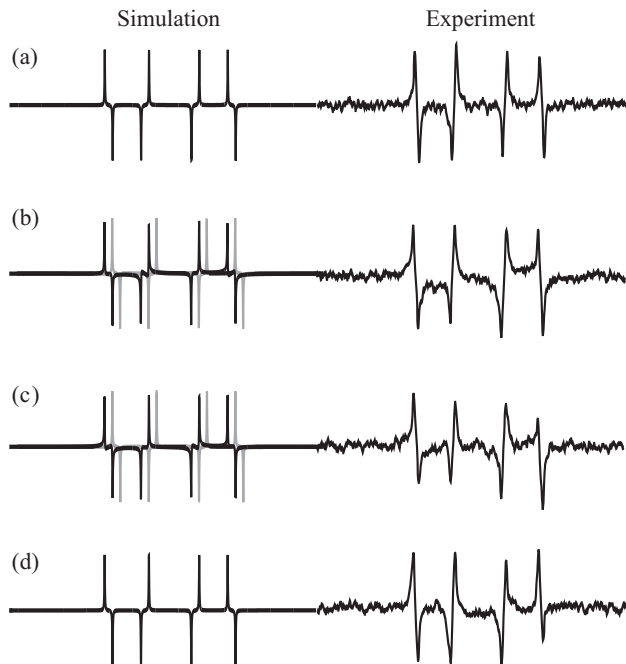


FIG. 11. We show the anti-phase signal of the spin of  $^{19}\text{F}$  with respect to the spins of  $^1\text{H}$ ,  $^{13}\text{C}$ , and  $^{15}\text{N}$  of a four-spin system corresponding to the simulation (left) and experiment (right). We use the conventional pulse sequence (a) ( $t_p = 64.4$  ms), an analytical pulse sequence (b) ( $t_p = 53.9$  ms), a pulse which was numerically-optimized for the abstract linear spin chain with rf controls on the second and third spin (c) ( $t_p = 53.2$  ms), and a pulse which was numerically-optimized for the more generally-coupled spin system with rf controls on all spins (d) ( $t_p = 54.0$  ms). The simulation for the abstract linear spin chain is given in gray color. All the other plots for the more realistic case of a more generally-coupled spin system are given in black color. The plots are scaled vertically by a factor of two.

tional pulse sequence corresponding to Fig. 11(a) while maintaining its robustness to additional couplings (see also Table VIII).

## VII. LINEAR SPIN CHAINS WITH MORE THAN FOUR SPINS

In this section, we generalize the numerical optimization of shaped pulses to linear spin chains of five and more spins. Figure 12 shows two examples of the optimized pulse shapes with coupling ratios  $k_\ell = 1$  and coupling strengths  $J_{\ell,\ell+1} = 88.05$  Hz. These examples suggest that time-optimal controls can be obtained on multiple spins even while irradiating only on the spins two to  $\ell - 1$  along the  $y$ -direction (cp. Sec. IV of Ref. [12]). We obtain shorter pulses for the numerically-optimized pulses compared to the conventional pulse sequences as summarized in Table VIII.

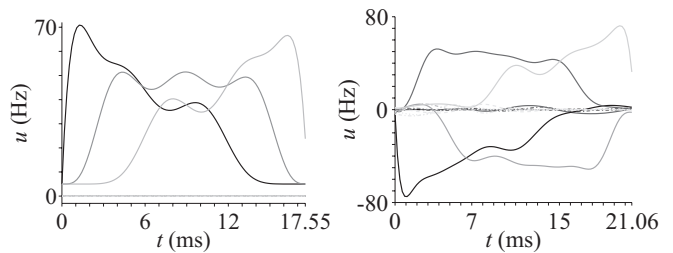


FIG. 12. Using all ten (or twelve) rf controls we determined numerically-optimized pulse shapes for linear spin chains of length five (or six) in the case of  $k = 1$ . We remark that most control strengths are very small.

TABLE VIII. We compare the minimum time  $t_p$  required for a coherence transfer by numerically-optimized (oc) and conventional (conv) pulse sequences for different number  $n$  of spins and coupling ratios  $k$ .

$n$	$t_p$ (s)					
	$k = 1$			$k \neq 1^a$		
	oc	conv	oc/conv	oc	conv	oc/conv
3	0.0098	0.0114	0.8596	0.0155	0.0177	0.8757
4	0.0138	0.0170	0.8118	0.0532	0.0644	0.8261
5	0.0177	0.0227	0.7797	–	–	–
6	0.0216	0.0284	0.7605	–	–	–

<sup>a</sup> For  $n = 3$  we have  $k = 1.59$ . And for  $n = 4$  we have  $k_1 = 2.38$  and  $k_2 = 0.94$ .

## VIII. CONCLUSION

In the case of linear three-spin chains we reproduced numerically the previous analytical results [11, 12] obtaining the same family of restricted controls by applying pulses only on the second spin along the  $y$ -axis. The same holds for linear four-spin chains where we also obtain the analytical family of restricted controls by applying pulses only on the second and third spin along the  $y$ -axis; but the numerically-optimized pulses appear to be a little shorter than the analytical ones. Both for three and four spins no gain in pulse duration is found if arbitrary pulse structures are allowed. These observations are summarized in Conjectures 1 and 2. Even for longer spin chains (consisting of up to six coupled spin-1/2) there is some numerical evidence suggesting that the same restricted controls motivated by Refs. [11, 12] lead to time-optimal pulses (in the case of unrestricted controls) for linear spin chains of arbitrary length.

Further numerical results are presented for more general and more realistic coupling topologies, for which so far no analytical results are known. Compared to linear spin chains we obtain different pulse structures depending on the number of available controls. We hope that the presented results and conjectures will motivate further analytical work in order to develop a better understanding of time-optimal control sequences for the generation

of multi-spin coherence.

Note that the minimum times for the transfers  $I_{1\delta} \rightarrow 2^{n-1}I_{1\epsilon_1} \cdots I_{n\epsilon_n}$  and  $2^{n-1}I_{1\epsilon_1} \cdots I_{n\epsilon_n} \rightarrow I_{1\delta}$  are identical ( $\delta, \epsilon_k \in \{x, y, z\}$  for  $k = 1, \dots, n$ ), which is directly relevant for “out and back” experiments and the reconversion of multiple-quantum coherence to detectable single quantum operators. In the experimental part, we demonstrated that the optimized pulse sequences work in realistic settings under relaxation and experimental imperfections (e.g. inhomogeneity of the control field, miscalibrations, and phase transients). In addition, the pulses can be made broadband (i.e. robust with respect to frequency offsets) using the DANTE approach.

Here we assumed for simplicity that each spin-1/2 can be selectively addressed, which is directly relevant to heteronuclear spin systems but the optimal transfer scheme can also be adapted to homonuclear spin systems. The presented sequences can be directly applied to small molecules and peptides, which is in particular true for the broadband versions. The minimum pulse sequence durations for complete transfer are reduced by up to 24% compared to conventional approaches (see Table VIII). Conversely, for a fixed transfer time signif-

icantly improved transfer amplitudes are possible, e.g., for a linear three-spin chain we gain approximately 23% in transfer efficiency when we allow only for half of the transfer time necessary for a complete transfer (cp. Fig. 7). For large proteins, further gains in efficiency are expected if relaxation-optimized pulse sequences can be developed for the specific relaxation super operator given in the system. Although such sequences are beyond the scope of the present paper, the results on time-optimal sequences presented here provide an important benchmark for relaxation-optimized sequences.

## ACKNOWLEDGMENTS

MN would like to thank the TUM Graduate school. RZ is supported by the Deutsche Forschungsgemeinschaft through the grant SCHU 1374/2-1. SJG acknowledges support from the DFG (GL 203/6-1), SFB 631, the EU program Q-ESSENCE, and the Fonds der Chemischen Industrie. We acknowledge the support by the Bayerisches NMR Zentrum, München.

- 
- [1] E. Lieb, T. Schultz, and D. Mattis, *Ann. Phys.* **18**, 407 (1961).
- [2] H. M. Pastawski, G. Usaj, and P. R. Levstein, *Chem. Phys. Lett.* **261**, 329 (1996).
- [3] S. J. Glaser and G. P. Drobny, *Chem. Phys. Lett.* **181**, 553 (1991).
- [4] J. Listerud, S. J. Glaser, and G. P. Drobny, *Mol. Phys.* **78**, 629 (1993).
- [5] S. J. Glaser, *J. Magn. Reson. A* **104**, 283 (1993).
- [6] S. J. Glaser and J. J. Quant, in *Advances in Magnetic and Optical Resonance*, Vol. 19, edited by W. S. Warren (Academic Press, San Diego, 1996) pp. 59–252.
- [7] R. M. White, *Quantum Theory of Magnetism* (Springer, Berlin, 1983).
- [8] D. C. Mattis, *The Theory of Magnetism I, Statistics and Dynamics* (Springer, Berlin, 1988).
- [9] Z. L. Mádi, B. Brutscher, T. Schulte-Herbrüggen, R. Brüschweiler, and R. R. Ernst, *Chem. Phys. Lett.* **268**, 300 (1997).
- [10] N. Khaneja and S. J. Glaser, *Phys. Rev. A* **66**, 060301(R) (2002).
- [11] H. Yuan, S. J. Glaser, and N. Khaneja, *Phys. Rev. A* **76**, 012316 (2007).
- [12] H. Yuan, R. Zeier, and N. Khaneja, *Phys. Rev. A* **77**, 032340 (2008).
- [13] F. Yamaguchi and Y. Yamamoto, *Appl. Phys. A* **68**, 1 (1999).
- [14] S. G. Schirmer and P. J. Pemberton-Ross, *Phys. Rev. A* **80**, 030301(R) (2009).
- [15] M. L. Remerowski, S. J. Glaser, and G. P. Drobny, *Mol. Phys.* **68**, 1191 (1989).
- [16] H. L. Eaton, S. W. Fesik, S. J. Glaser, and G. P. Drobny, *J. Magn. Reson.* **90**, 452 (1990).
- [17] J. Cavanagh, W. J. Fairbrother, A. G. Palmer, and N. J. Skelton, *Protein NMR Spectroscopy: Principles and Practice* (Academic Press, San Diego, 1996).
- [18] R. R. Ernst, G. Bodenhausen, and A. Wokaun, *Principles of Nuclear Magnetic Resonance in One and Two Dimensions* (Clarendon Press, Oxford, 1997) reprinted with corrections.
- [19] S. J. Archer, M. Ikura, D. A. Torchia, and A. Bax, *J. Magn. Reson.* **95**, 636 (1991).
- [20] M. Sattler, J. Schleucher, and C. Griesinger, *Prog. NMR Spec.* **34**, 93 (1999).
- [21] M. H. Levitt and R. R. Ernst, *J. Chem. Phys.* **83**, 3297 (1985).
- [22] E. Ising, *Z. Physik* **31**, 253 (1925).
- [23] W. J. Caspers, *Spin systems* (World Scientific, Singapore, 1989).
- [24] G. A. Morris and R. Freeman, *J. Am. Chem. Soc.* **101**, 760 (1979).
- [25] N. Khaneja, R. Brockett, and S. J. Glaser, *Phys. Rev. A* **63**, 032308 (2001).
- [26] T. O. Reiss, N. Khaneja, and S. J. Glaser, *J. Magn. Reson.* **154**, 192 (2002).
- [27] N. Khaneja, S. J. Glaser, and R. Brockett, *Phys. Rev. A* **65**, 032301 (2002).
- [28] N. Khaneja, F. Kramer, and S. J. Glaser, *J. Magn. Reson.* **173**, 116 (2005).
- [29] N. Khaneja, B. Heitmann, A. Spörl, H. Yuan, T. Schulte-Herbrüggen, and S. J. Glaser, *Phys. Rev. A* **75**, 012322 (2007).
- [30] R. Fisher, H. Yuan, A. Spörl, and S. Glaser, *Phys. Rev. A* **79**, 042304 (2009).
- [31] E. Assémat, M. Lapert, Y. Zhang, M. Braun, S. J. Glaser, and D. Sugny, *Phys. Rev. A* **82**, 013415 (2010).
- [32] N. Khaneja, T. Reiss, B. Luy, and S. J. Glaser, *J. Magn. Reson.* **162**, 311 (2003).

- [33] N. Khaneja, B. Luy, and S. J. Glaser, Proc. Natl. Acad. Sci. USA **100**, 13162 (2003).
- [34] D. Stefanatos, N. Khaneja, and S. J. Glaser, Phys. Rev. A **69**, 022319 (2004).
- [35] D. P. Fröh, T. Ito, J.-S. Li, G. Wagner, S. J. Glaser, and N. Khaneja, J. Biomol. NMR **32**, 23 (2005).
- [36] D. Stefanatos, N. Khaneja, and S. J. Glaser, Phys. Rev. A **72**, 062320 (2005).
- [37] M. Lapert, Y. Zhang, M. Braun, S. J. Glaser, and D. Sugny, Phys. Rev. Lett. **104**, 083001 (2010).
- [38] N. C. Nielsen, C. Kehlet, S. J. Glaser, and N. Khaneja, Encyclopedia of Nuclear Magnetic Resonance **9**, 100 (2010).
- [39] T. E. Skinner, T. O. Reiss, B. Luy, N. Khaneja, and S. J. Glaser, J. Magn. Reson. **163**, 8 (2003).
- [40] K. Kobzar, B. Luy, N. Khaneja, and S. J. Glaser, J. Magn. Reson. **173**, 229 (2005).
- [41] K. Kobzar, T. E. Skinner, N. Khaneja, S. J. Glaser, and B. Luy, J. Magn. Reson. **194**, 58 (2008).
- [42] N. I. Gershenzon, T. E. Skinner, B. Brutscher, N. Khaneja, M. Nimbalkar, B. Luy, and S. J. Glaser, J. Magn. Reson. **192**, 235 (2008).
- [43] N. Khaneja, T. Reiss, C. Kehlet, T. Schulte-Herbrüggen, and S. J. Glaser, J. Magn. Reson. **172**, 296 (2005).
- [44] Z. Tošner, T. Vosegaard, C. T. Kehlet, N. Khaneja, S. J. Glaser, and N. C. Nielsen, J. Magn. Reson. **197**, 120 (2009).
- [45] S. Machnes, U. Sander, S. J. Glaser, P. de Fouquières, A. Gruslys, S. Schirmer, and T. Schulte-Herbrüggen, Phys. Rev. A **84**, 022305 (2011).
- [46] P. de Fouquieres, S. G. Schirmer, S. J. Glaser, and I. Kuprov, J. Magn. Reson. **212**, 241 (2011).
- [47] A. N. Pechen and D. J. Tannor, Phys. Rev. Lett. **106**, 120402 (2011).
- [48] M. Lapert, Y. Zhang, M. Braun, S. J. Glaser, and D. Sugny, Phys. Rev. A **82**, 063418 (2010).
- [49] K. Kobzar, T. E. Skinner, N. Khaneja, S. J. Glaser, and B. Luy, J. Magn. Reson. **170**, 236 (2004).
- [50] J. L. Neves, B. Heitmann, T. O. Reiss, H. H. R. Schor, N. Khaneja, and S. J. Glaser, J. Magn. Reson. **181**, 126 (2006).
- [51] N. Pomplun, B. Heitmann, N. Khaneja, and S. J. Glaser, Appl. Magn. Reson. **34**, 331 (2008).
- [52] N. Pomplun and S. J. Glaser, Phys. Chem. Chem. Phys. **12**, 5791 (2010).
- [53] M. Braun and S. J. Glaser, J. Magn. Reson. **207**, 114 (2010).
- [54] N. I. Gershenzon, K. Kobzar, B. Luy, S. J. Glaser, and T. E. Skinner, J. Magn. Reson. **188**, 330 (2007).
- [55] M. Lapert, Y. Zhang, S. J. Glaser, and D. Sugny, J. Phys. B **44**, 154014 (2011).
- [56] Y. Zhang, M. Lapert, D. Sugny, M. Braun, and S. J. Glaser, J. Chem. Phys. **134**, 054103 (2011).
- [57] T. E. Skinner, T. O. Reiss, B. Luy, N. Khaneja, and S. J. Glaser, J. Magn. Reson. **167**, 68 (2004).
- [58] T. E. Skinner, K. Kobzar, B. Luy, R. Bendall, W. Bermel, N. Khaneja, and S. J. Glaser, J. Magn. Reson. **179**, 241 (2006).
- [59] T. E. Skinner, M. Braun, K. Woelk, N. I. Gershenzon, and S. J. Glaser, J. Magn. Reson. **209**, 282 (2011).
- [60] G. A. Morris and R. Freeman, J. Magn. Reson. **29**, 433 (1978).
- [61] N. Khaneja, J.-S. Li, C. Kehlet, B. Luy, and S. J. Glaser, Proc. Natl. Acad. Sci. USA **101**, 14742 (2004).
- [62] N. Pomplun, PhD thesis, Technische Universität München (2010).
- [63] R. Marx, N. Pomplun, W. Bermel, H. Zeiger, F. Engelke, A. F. Fahmy, and S. J. Glaser, “Engineering of an all-heteronuclear 5-qubit NMR quantum computer,” in preparation (2011).
- [64] D. Canet, J. Brondeau, and C. Roumestand, J. Magn. Reson. A **117**, 103 (1995).
- [65] M. H. Levitt, R. Freeman, and T. Frenkiel, J. Magn. Reson. **47**, 328 (1982).